DOI: 10.1002/marc.((insert number)) ((or ppap., mabi., macp., mame., mren., mats.))

Communication

Needle-less electrohydrodynamic co-jetting of bicompartmental particles and fibers from an extended fluid interface[a]

Jacob H. Jordahl, Stacy Ramcharan, Jason V. Grergory, Joerg Lahann*

J.H. Jordahl, S. Ramcharan, J.V. Gregory, and Prof. J. Lahann

Biointerfaces Institute, Department of Chemical Engineering

University of Michigan

2800 Plymouth Rd, Ann Arbor, MI 48109, USA

Ann Arbor, MI, 48109

Prof. J. Lahann

Department of Biomedical Engineering, Material Science and Engineering, and Macromolecular Science and Engineering

University of Michigan

[a] **Supporting Information** is available online from the Wiley Online Library or from the author.

2800 Plymouth Rd, Ann Arbor, MI 48109, USA
E-mail: Lahann@umich.edu

Electrohydrodynamic co-jetting can result in fibers (electrospinning) and particles (electrospraying) with complex, bicompartmental architectures. An important consideration for application of bicompartmental particles and fibers is the limited throughput derived from the use of parallel capillaries which require laminar flow to form a multifluidic interface. Here, we report a novel

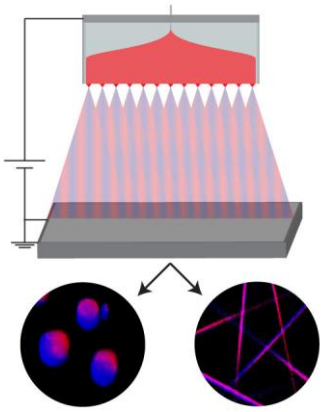

synthesis approach that takes advantage of an extended bicompartmental fluid interface formed at the sharp edge of a two-dimensional plate. Upon application of an electrical potential to the plate, several electrified fluid jets form spontaneously. Depending on the processing conditions, either bicompartmental particles or fibers with well-defined architectures are prepared. Importantly, this needle-less process yields production rates that are more than 30 times higher than those of conventional needle-based techniques. Fiber properties, such as morphology or size, are independent of the flow rate, indicating that this process is physically self-regulating by adjusting the number of jets ejecting from the extended fluid interface. The needle-less preparation of bicompartmental particles and fibers is an important technological breakthrough that can enable further advances ranging from drug delivery and tissue engineering to industrial applications.

1. Introduction

Electrospinning and electrospraying have become technological approaches for creating particles and fibers on small length scales, e.g., dimensions ranging from microns to nanometers in size.[1-3] These techniques typically involve the transport of polymer solutions through a metal capillary. Upon application of a critical voltage, the droplet at end of the metal capillary is distorted into a Taylor cone, and a fluid jet is emitted from the cone apex.[2] While the fluid jet traverses towards a grounded electrode it can either break up into droplets, i.e., electrospraying,[4, 5] or is stretched into a fiber, i.e., electrospinning.[6] This technology has been implemented in a variety of applications ranging from chemical sensors,[7, 8] filtration membranes,[9, 10] and tissue engineering [10-13] using electrospinning, to drug delivery vehicles [5, 14] and microencapsulation.[15]

More recently, the development of electrohydrodynamic (EHD) co-jetting,[16] which imparts multiple chemical functionalities within distinct compartmental domains of both particles and fibers, has shown great promise in creating more complex drug delivery platforms[17-19] as well as patterned targeting domains.[20, 21] Additionally, multicomponent fibers have shown promise in creating next-generation tissue engineering constructs [22-24] and stimuli-responsive micro- and nanoactuators.[25-27] Scaling this technology to gram scale production has been difficult due to the limitation of one fluid jet per co-jetting setup, potentially limiting the commercial viability and widespread adaptation of this technique.

In the case of conventional electrospinning, the limited scalability has been addressed through the development of needle-less jetting processes which can produce fibers at rates orders of magnitude greater than what is possible with a single capillary.[28-32] In principal, needle-less electrospinning is based on the spontaneous ejection of multiple jets from a fluid reservoir in response to the application of sufficiently high electrical potentials. While this approach has been

very successful for conventional electrospinning, it is not directly translatable to electrohydrodynamic co-jetting, because the latter requires controlled co-flow of two fluids prior to jet formation. Herein, we describe a needle-less electrospinning and electrospraying technology which allows for the fabrication of bicompartmental fibers and particles.

2. Experimental Section

2.1 Materials

Poly(D,L-lactic-co-glycolic acid) (PLGA, MW 50-75 kg mol^{-1}), poly(vinyl acetate) (PVAc, MW 113 kg mol^{-1}), poly[(m-phenylenevinylene)-alt-(2,5-dihexyloxy-p-phenylenevinylene)] (PMPDHPV), tetrahydrofuran (THF), chloroform, and N,N-dimethylformamide (DMF) were purchased from Sigma Aldrich. Methoxy-polyethylene glycol (PEG)-rhodamine (MW 5 kg mol^{-1}) was purchased from Creative PEG Works.

2.2. Device design

The microchannel EHD co-jetting device was fabricated from 316 stainless steel to an overall size of 76.4 x 25.5 (length x width). A 0.35 mm microchannel was created on each side of a 0.7 mm thick plate by placing a raised edge on both sides of the device. The top of the device contained a 2 mm tall and 3.25 mm wide ridge, designed for glass slides to mount flush to the device. Fluid inlets were placed on both sides of the metal plate and were centered lengthwise on the ridge of the

device. The plate edge at the outlet of the microchannels was sharpened to a point, and grooves were placed approximately every 1 mm along the edge to aid in fluid flow. Glass slides were cut to size and were mounted onto the device.

2.3 Particle and fiber preparation

Bicompartmental particles were fabricated using two 6.5 wt% solutions of PLGA dissolved in a 97:3 ratio of chloroform:DMF. One of the solutions contained 30 μg ml^{-1} of PMPDHPV, while the second solution contained 30 μg ml^{-1} of mPEG-Rhodamine. Each solution was pumped at flow rates ranging from 1.0 to 13.2 ml hr^{-1} (for a total flow rate of 2.0 to 26.4 ml hr^{-1}) into the microchannel device, and a 60 kV electric potential was applied once solution emerged from the microchannels. Flow rates reported represent flow of each individual component. The total flow rate through the device is twice what is reported unless otherwise specified.

Bicompartmental fibers were fabricated using two 35 wt% solutions of PLGA dissolved in a 1:1 ratio of chloroform:DMF containing similar dye concentrations as the particles. Each solution was pumped into the microchannels at a flow rate of 13.2 ml hr^{-1}, for a total of 26.4 ml hr^{-1}, at an applied electric potential of 75 kV.

Bicompartmental fibers were created by flowing PLGA and PVAc polymer solutions on either side of the microchannel EHD co-jetting device. A 35 wt% PLGA solution in a 1:1 THF to DMF solvent system was co-spun with a 35 wt% PVAc solution in a 6:4 chloroform to DMF solvent system. Total flow rates of 2 to 26.4 ml hr^{-1} were utilized at a tip to ground distance of 40 cm and an applied electric potential of 75 kV.

Scanning electron microscopy of the particles was performed using an FEI Helios SEM/FIB, while fibers were imaged using an AMRAY 1910 Field Emission Scanning Electron Microscope (FEG-SEM). Fiber diameter histograms were determined by ImageJ using the DiameterJ plugin, an approach previously reported literature.[33] In this process, grayscale images were segmented using an automated thresholding technique. The threshold setting M7 was used for all subsequent analysis.

Fluorescence imaging was conducted with a Nikon A-1 inverted confocal laser scanning microscope (CLSM) using a 60x oil immersion objective with violet corrected lens, and were processed on Imaris (Version 7.5) software. Particle size distributions were determined by measuring all the particles across 140 x 240 µm quadrants in nine separate fields of view. Particle anisotropy was determined by counting all the particles containing either one or two compartments within nine 3D fields of view within a confocal z-stack. Particles viewed from this perspective could be easily distinguished from one another. Relative compartmental ratios were computed by generating surfaces which encapsulated the volume of each compartment in Imaris. The volume of each surface on the particle was measured, providing a relative volume ratio for each component.

3. Results and Discussion

3.1 Device Design

Currently, electrohydrodynamic (EHD) co-jetting requires the use of two capillaries in parallel to create fibers or particles with two or more compartments (**Figure 1 A**).[16] To scale this technology, complex experimental setups involving multiple dual capillary orifices are required.

Here, an alternative strategy is explored that relies on the ejection of multiple jets from the edge of an appropriately designed metal plate. Two fluids flow on opposite sides of the plate and combine at the edge to form a stable fluid interface (**Figure 1 B**). It was hypothesized that this elongated fluid interface would act similarly to the droplet interface which is formed by the dual capillaries typically used in EHD co-jetting; and that upon application of high voltage spontaneous formation of multiple fluid jets would spontaneously form along the extended fluid interface.

Schematic representations of the top (inlet) and bottom (outlet) of the device show the location of the two microchannels relative to one another, as well as the location of the fluid inlet ports (**Figure 1 C**). Pumping the fluids into the fluid inlet ports of the assembled device allows for the polymer solutions to move on opposite sides of the metal plate. Once the device is filled, a fluid interface is formed at the lower edge. Upon formation of the fluid interface, a high electric potential is applied to the device, forming multiple Taylor cones along the device outlet (**Movie S 1**). The fluid jets formed from the device are then accelerated towards a grounded electrode, where the final particles or fibers are collected and subsequently analyzed (**Figure 1 D, Movie S 2**).

3.2 Bicompartmental particle preparation

For microparticle fabrication, the needle-less co-jetting device was infused with two 6.5 wt% PLGA solutions containing different dyes. Each PLGA solution was infused at flow rates ranging from 2.0 ml hr^{-1} to 26.4 ml hr^{-1} to determine the optimum flow rate for bicompartmental particle preparation. For each flow rate, an electric potential of 60 kV was applied to the device. The distance between tip and grounded collector was held constant at 40 cm. It was observed that as the flow

rate increased, an increasing number of Taylor cones were formed to maintain a steady state of particle production. The number of Taylor cones increased from three at a 2.0 ml hr^{-1} flow rate, to seven at a flow rate of 26.4 ml hr^{-1} along the 7 cm outlet.

Visualization of the bicompartmental particles was performed using confocal laser scanning microscopy (CLSM). Z-stack imaging was utilized to reconstruct the 3D structure of the resultant particles (**Figure 2 A, B**). Analysis of the particles in the z-stack images revealed that at a flow rate of 2.0 ml hr^{-1}, 96.5% of the particles featured two clearly distinguishable compartments. Within these particles, it was determined that the relative ratio of each compartment was 50.8% ± 4.5% (n=150). This compares well with the yields described for needle-based co-jetting.[34, 35] Moreover, statistical analysis of the images obtained by confocal microscopy yielded particle size distributions for the particles prepared with a flow rate of 2.0 ml hr^{-1} (**Figure 2 D**). For comparison, electrohydrodynamic co-jetting of the same polymer solution using parallel capillaries requires a total flow rate of 0.4 ml hr^{-1} (0.2 ml hr^{-1} for each component) to obtain a stable cone-jet. Under otherwise unaltered conditions, the resultant particles had size distributions and particle morphologies that matched the ones observed for needle-less jetting seen in Figure 2 D (see **Figure S 1** for comparison).

Not surprisingly, the flow rate had an important influence on particle morphologies: Bicompartmental particles prepared by needle-less co-jetting ranged from close-to-perfect spherical particles at lower flow rates (**Figure 2 C**) to flattened discs at higher flow rates (**Figure S 2**). A distribution of discs and particles were observed at flow rates as high as 20 ml hr^{-1}, and discs and red-blood cell shaped particles were predominantly observed for flow rates above 26.4 ml hr^{-1}. We note that disc-shaped particles are generally seen for polymer solutions pumped at low concentrations at higher flow rates.[34, 36] The formation of discs can typically be avoided when the tip to grounded collector distance is increased. At even higher flow rates, the increased solvent

concentration in the atmosphere around the depositing particles leads to a slower evaporation rate which hinders the solidification of the particle, causing it to flatten into a disc shape.[36] These disc shaped particles prepared by needle-less co-jetting were found to still retain a bicompartmental character (**Figure S 3**).

3.3 Bicompartmental fiber preparation

Infusion of the microchannel device with two 35 wt% PLGA solutions, each loaded with a different colored fluorescent dye, resulted in the formation of micron to sub-micron sized fibers upon application of a 75 kV electric potential. Again, flow rates from 2.0 ml hr^{-1} to 26.4 ml hr^{-1} were examined to determine maximum production rate of bicompartmental fiber mats, and how flow rate affects the overall fiber morphology. For all fiber jetting experiments, the tip to grounded collector distance was maintained at 40 cm with a constant applied electric potential. Similar increases in Taylor cone numbers with increasing flow rates were observed during fiber electrospinning. However, these cones were more dynamic in nature, and their numbers varied with time. At flow rates of 2.0 ml hr^{-1}, one to three Taylor cones formed along the outlet of the device, and increasing the flow rate to 26.4 ml hr^{-1} produced four to eight Taylor cones.

For all flow rates examined, bicompartmental fibers were obtained. Even at the highest flow rate, the reconstruction of CLSM z-stacks confirmed that the fibers maintained a bicompartmental architecture (**Figure 3 A, B**). CLSM imaging of the cross-sectional view of the fibers further confirms the presence of two distinct compartments (**Figure 3 B**). SEM micrographs reveal fibers with a contiguous, bead-free morphology across all flow rates examined (**Figure 3 C**). Under the conditions

used for needle-less co-jetting, fibers had an average diameter of 0.95 μm (**Figure 3 E**). Fibers formed at 2 ml hr^{-1} had a similar morphology and fiber size distribution as all other fibers, including the highest flow rates examined of 26.4 ml hr^{-1}. Comparison to fibers fabricated using standard needle-based co-jetting using identical PLGA solutions shows a similar fiber size distribution and morphology, demonstrating the stability of this method in fiber production (**Figure 3 D**). This was accomplished despite increasing the overall fiber production rate by over a factor of 30, from a total flow rate of 0.8 ml hr^{-1} in the case of needle-based electrospinning to over 26.4 ml hr^{-1} using a needle-less device.

Similar results were found when electrospinning two dissimilar materials. Co-jetting the PLGA solution with poly(vinyl acetate) (PVAc) using the needle-less device produced fibers with a bicompartmental architecture, with 95.5 ± 3.4% of the fibers containing two compartments when electrospun at the highest flow rate of 26.4 ml hr^{-1} (**Figure 4 A, B**). The fibers had a consistent bead-free morphology, and a similar fiber size distribution relative to each other and to standard needle-based electrospinning techniques (**Figure 4 C-E**) indicating the system is self-regulating, adding more or less Taylor cones as the flow rate is modulated.

These results demonstrate that fiber production rates of over 9 g hr^{-1} (over a 30 fold increase in production rate), well over an order of magnitude higher than typical bicompartmental fiber electrospinning (approximately 0.2 g hr^{-1}), can be achieved using this novel needle-less co-jetting technology. This results were consistent for both, fibers loaded with the same base polymer (PLGA) and two different additives (dyes) as well as for fibers comprised of entirely different base polymers (PLGA/PVAc). Further increases in fiber production rate may be feasible, if higher flow rates can be achieved. Increasing the length of the extended edge used to stabilize the fluid interface would also provide a means of further increasing the rate of production of fibers.

4. Conclusions

Bicompartmental particles and fibers, as well as bicomponent fibers containing different base polymers, were successfully fabricated using a newly developed needle-less EHD co-jetting technique. The device was designed to accommodate two independent fluid flows, which would combine to form a uniform fluid interface at the outlet of a microchannel. Application of a high electric field led to spontaneous formation of several distinct Taylor cones along the fluid interface, resulting in the deposition of bicompartmental fibers and particles. Production rates of fibers were calculated to be on the order of 9 g hr^{-1}, which is over 30 times higher than standard electrospinning approaches. Spherical particles also had increased production rates, around five times higher than needle-based EHD co-jetting. Other bicompartmental particle geometries are also accessible, including discs, which could be fabricated at a rate of nearly 2 g hr^{-1}. Scaling this technology using larger fluid interfaces and higher flow rates will be examined in future work. This technique provides a potential means for scaling up EHD co-jetted particles and fibers for commercial applications.

Supporting Information

Supporting Information is available from the Wiley Online Library

Acknowledgements

The authors would like to acknowledge funding from the Defense Threat Reduction Agency (HDTRA-1-15-1-0045). J.H.J. acknowledges the support of NIH's Microfluidics in Biomedical Sciences Training Program: NIH NIBIB T32 EB005582. S.R. acknowledges the Rackham Graduate School for funding provided by the Rackham Merit Fellowship.

Received: Month XX, XXXX; Revised: Month XX, XXXX; Published online:

((For PPP, use "Accepted: Month XX, XXXX" instead of "Published online")); DOI: 10.1002/marc.((insert number)) ((or ppap., mabi., macp., mame., mren., mats.))

Keywords: High-throughput synthesis, electrospinning, electrospraying, Janus particles, Janus fibers, microfluidics

References

[1] I. K. Kwon, S. Kidoaki, T. Matsuda, *Biomaterials* **2005**, *26*, 3929.

[2] D. H. Reneker, I. Chun, *Nanotechnology* **1996**, *7*, 216.

[3] A. Greiner, J. H. Wendorff, *Angew Chem Int Edit* **2007**, *46*, 5670.

[4] M. Cloupeau, B. Prunetfoch, *J Aerosol Sci* **1994**, *25*, 1021.

[5] J. W. Xie, L. K. Lim, Y. Y. Phua, J. S. Hua, C. H. Wang, *J Colloid Interf Sci* **2006**, *302*, 103.

[6] D. H. Reneker, A. L. Yarin, H. Fong, S. Koombhongse, *J Appl Phys* **2000**, *87*, 4531.

[7] M. S. Kwon, J. H. Jordahl, A. W. Phillips, K. Chung, S. Lee, J. Gierschner, J. Lahann, J. Kim, *Chem Sci* **2016**, *7*, 2359.

[8] X. Y. Wang, C. Drew, S. H. Lee, K. J. Senecal, J. Kumar, L. A. Sarnuelson, *Nano Lett* **2002**, *2*, 1273.

[9] P. Gibson, H. Schreuder-Gibson, D. Rivin, *Colloid Surface A* **2001**, *187*, 469.

[10] Z. M. Huang, Y. Z. Zhang, M. Kotaki, S. Ramakrishna, *Compos Sci Technol* **2003**, *63*, 2223.

[11] W. J. Li, C. T. Laurencin, E. J. Caterson, R. S. Tuan, F. K. Ko, *J Biomed Mater Res* **2002**, *60*, 613.

[12] T. J. Sill, H. A. von Recum, *Biomaterials* **2008**, *29*, 1989.

[13] H. Yoshimoto, Y. M. Shin, H. Terai, J. P. Vacanti, *Biomaterials* **2003**, *24*, 2077.

[14] S. Chakraborty, I. C. Liao, A. Adler, K. W. Leong, *Adv Drug Deliver Rev* **2009**, *61*, 1043.

[15] I. G. Loscertales, A. Barrero, I. Guerrero, R. Cortijo, M. Marquez, A. M. Ganan-Calvo, *Science* **2002**, *295*, 1695.

[16] K. H. Roh, D. C. Martin, J. Lahann, *Nat Mater* **2005**, *4*, 759.

[17] S. Rahmani, C. H. Villa, A. F. Dishman, M. E. Grabowski, D. C. Pan, H. Durmaz, A. C. Misra, L. Colon-Melendez, M. J. Solomon, V. R. Muzykantov, J. Lahann, *J Drug Target* **2015**, *23*, 750.

[18] E. Sokolovskaya, S. Rahmani, A. C. Misra, S. Brase, J. Lahann, *Acs Appl Mater Inter* **2015**, *7*, 9744.

[19] S. Rahmani, T. H. Park, A. F. Dishman, J. Lahann, *J Control Release* **2013**, *172*, 239.

[20] S. Rahmani, A. M. Ross, T. H. Park, H. Durmaz, A. F. Dishman, D. M. Prieskorn, N. Jones, R. A. Altschuler, J. Lahann, *Adv Healthc Mater* **2016**, *5*, 94.

[21] S. Rahmani, S. Saha, H. Durmaz, A. Donini, A. C. Misra, J. Yoon, J. Lahann, *Angew Chem Int Edit* **2014**, *53*, 2332.

[22] S. Bhaskar, K. H. Roh, X. W. Jiang, G. L. Baker, J. Lahann, *Macromol Rapid Comm* **2008**, *29*, 1973.

[23] S. Mandal, S. Bhaskar, J. Lahann, *Macromol Rapid Comm* **2009**, *30*, 1638.

[24] J. Yoon, T. W. Eyster, A. C. Misra, J. Lahann, *Adv Mater* **2015**, *27*, 4509.

[25] J. Lee, T. H. Park, K. J. Lee, J. Lahann, *Macromol Rapid Comm* **2016**, *37*, 73.

[26] S. Saha, D. Copic, S. Bhaskar, N. Clay, A. Donini, A. J. Hart, J. Lahann, *Angew Chem Int Edit* **2012**, *51*, 660.

[27] K. J. Lee, J. Yoon, S. Rahmani, S. Hwang, S. Bhaskar, S. Mitragotri, J. Lahann, *P Natl Acad Sci USA* **2012**, *109*, 16057.

[28] A. L. Yarin, E. Zussman, *Polymer* **2004**, *45*, 2977.

[29] B. A. Lu, Y. J. Wang, Y. X. Liu, H. G. Duan, J. Y. Zhou, Z. X. Zhang, Y. Q. Wang, X. D. Li, W. Wang, W. Lan, E. Q. Xie, *Small* **2010**, *6*, 1612.

[30] N. M. Thoppey, J. R. Bochinski, L. I. Clarke, R. E. Gorga, *Polymer* **2010**, *51*, 4928.

[31] X. Wang, H. T. Niu, T. Lin, X. G. Wang, *Polym Eng Sci* **2009**, *49*, 1582.

[32] K. M. Forward, G. C. Rutledge, *Chem Eng J* **2012**, *183*, 492.

[33] N. A. Hotaling, K. Bharti, H. Kriel, C. G. Simon, *Biomaterials* **2015**, *61*, 327.

[34] S. Bhaskar, K. M. Pollock, M. Yoshida, J. Lahann, *Small* **2010**, *6*, 404.

[35] M. Yoshida, K. H. Roh, S. Mandal, S. Bhaskar, D. W. Lim, H. Nandivada, X. P. Deng, J. Lahann, *Adv Mater* **2009**, *21*, 4920.

[36] N. Bock, M. A. Woodruff, D. W. Hutmacher, T. R. Dargaville, *Polymers-Basel* **2011**, *3*, 131.

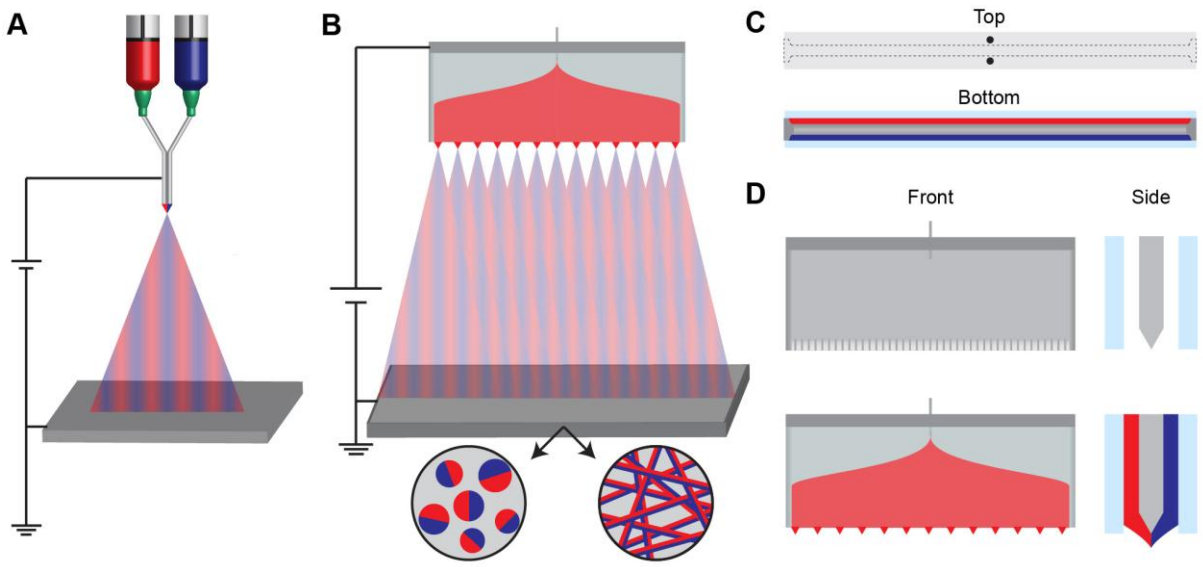

Figure 1. A) A standard EHD co-jetting experimental setup includes a single syringe pump, which dispenses two fluids simultaneously through two parallel capillaries. A high voltage is applied to the dual-capillaries, resulting in either electrospinning or electrospraying of bicompartmental fibers or particles respectively. Scaling up this process would require many capillaries in parallel, which is fundamentally impractical. B) A needle-less co-jetting technique would allow for an increased cone density with high flow rates using a relatively simple design.Operation of this device with results in the deposition of particles or fibers with multiple compartmentalized domains. C) A top and bottom view of the device showing glass slides spaced away from a center plate via raised edges on either side. This creates microchannels for the fluid to flow through. D) The device itself consists of a center plate which is sharpened to an edge to stabilize a biphasic fluid interface with glass walls on either side. Filling the device with polymer solution on either side leads to the formation of an extended fluid interface. Application of electric potential leads to the formation of multiple bicomponent Taylor cones (Movie S 1).

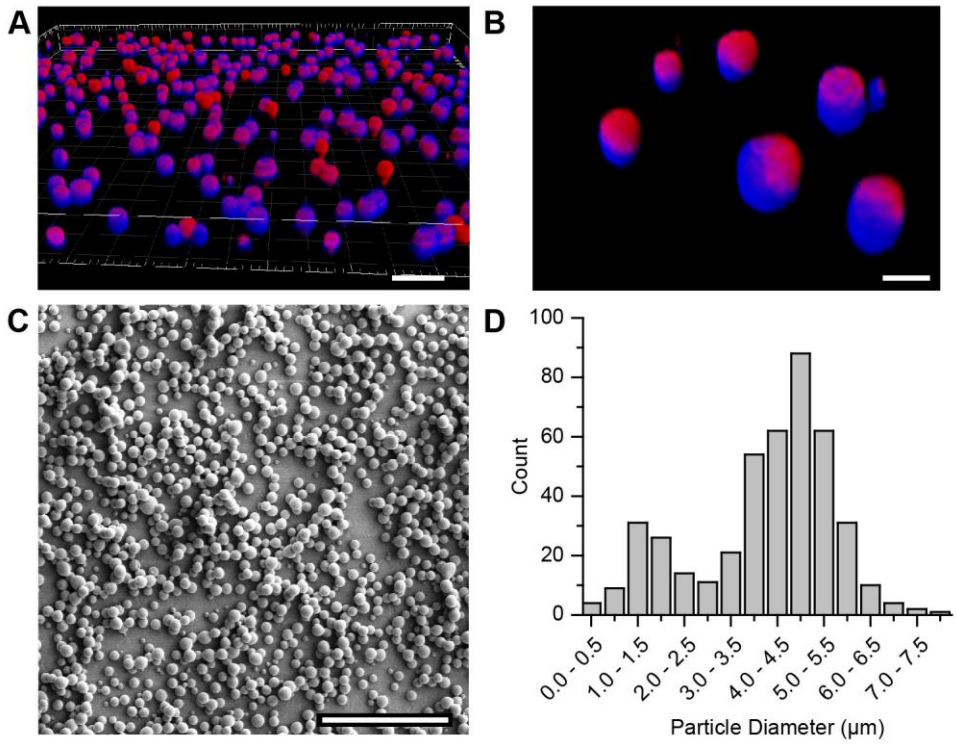

Figure 2. Bicompartmental particles composed of PLGA loaded with different fluorescent dyes fabricated via needle-less EHD co-jetting device. A) Confocal laser scanning microscopy was used to verify the bicompartmental nature of the particles. B) A zoomed in image of these particles highlights the bicompartmental nature of these particles. C) Scanning electron micrograph of particles fabricated using this device show particle morphology is consistent with previous EHD co-jetting capabilities. D) The particle size distribution as calculated from nine different fields of view via confocal microscopy validates these observations (see Fig. S 2). Scale bars indicate 20 µm (A), 5 µm (B), 50 µm (C).

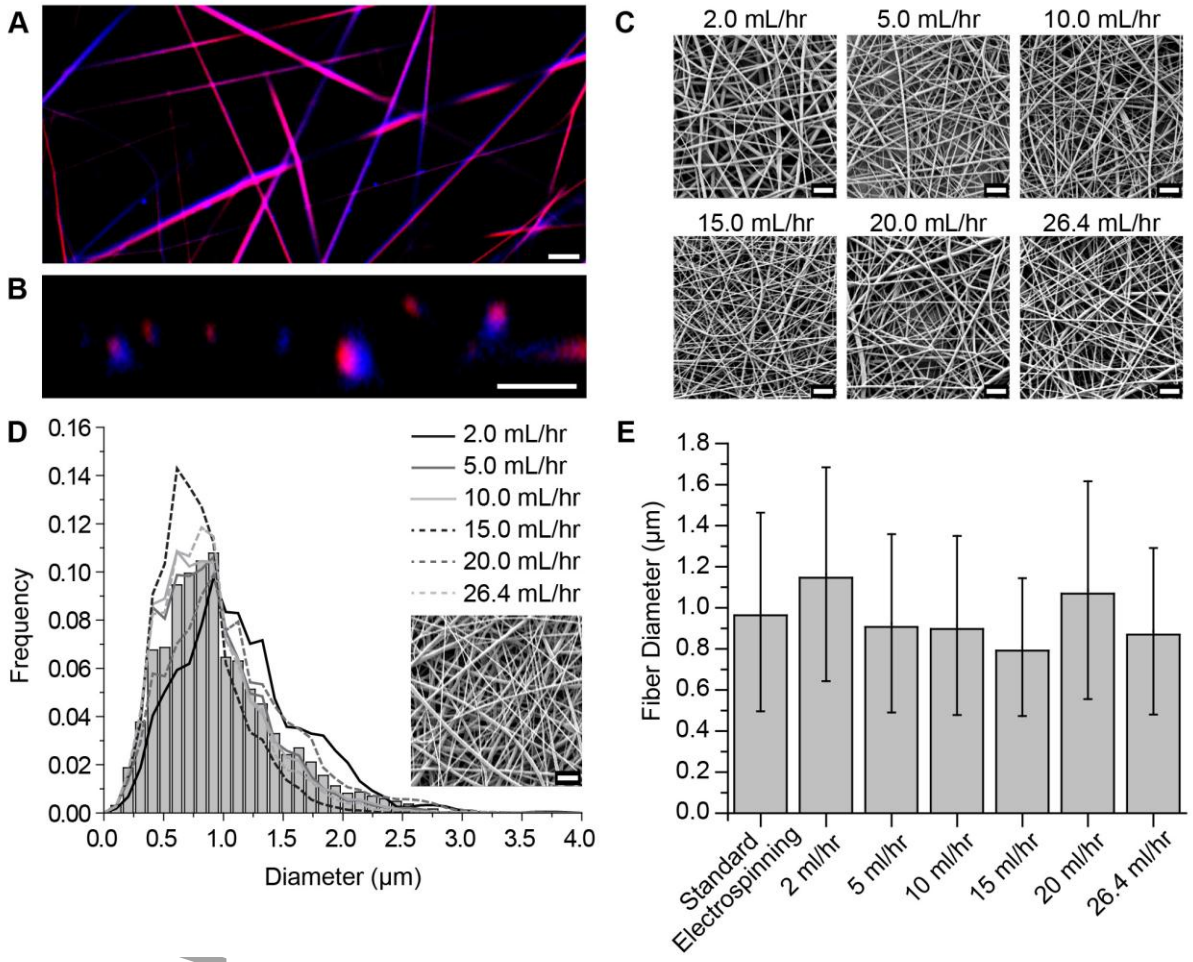

Figure 3. Bicompartmental fibers composed of PLGA compartments loaded with different dyes as fabricated via needle-less EHD co-jetting device. A) Confocal laser scanning microscopy verifies the bicompartmental fiber architecture is maintained after being processed by the microchannel EHD co-jetting device, even at flow rates of 26.4 ml hr^{-1}. B) A representative cross sectional view of the fibers shown in (A) highlights the two compartments present within the fibers. C) Scanning electron microscopy of fibers produced from 2 to 26.4 ml hr^{-1} show a bead free morphology which is similar at each respective flow rate. D) A histogram of fiber diameters from fibers spun in a standard side-by-side capillary (SEM shown in inset) is compared to the fiber size distributions of the fibers produced using the microchannel EHD co-jetting device at different flow rates, as indicated by the respective lines. E) Average fiber diameter is shown for each of the samples, showing the fiber size is consistent for each condition. Error bars indicate standard deviations. Scale bars indicate 10 μm (A-D).

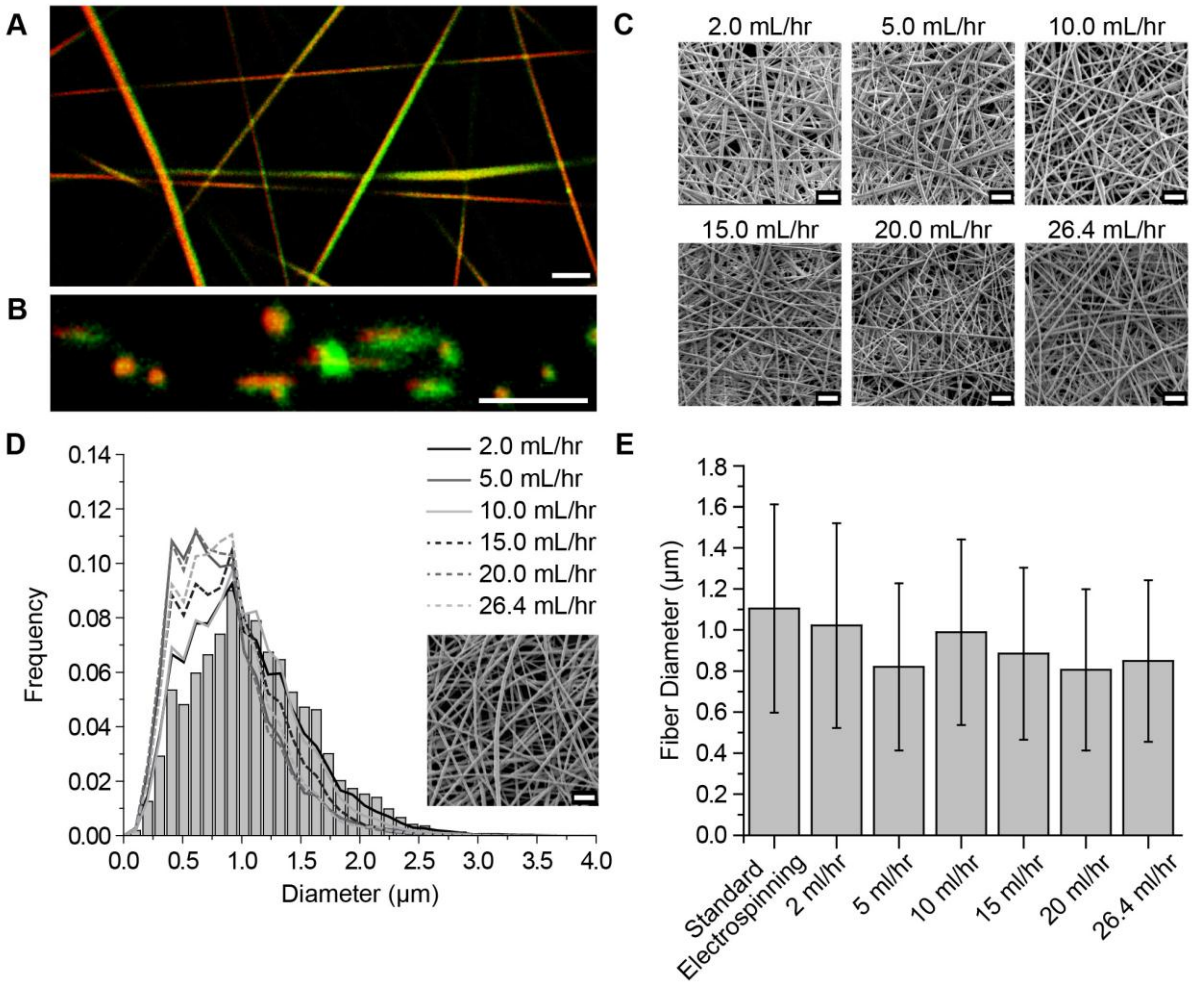

Figure 4. Bicomponent fibers with one compartment containing PLGA (red) and the second containing PVAc (green) were loaded with different dyes and fabricated via needle-less EHD co-jetting device. A) Confocal laser scanning microscopy verifies the bicompartmental fiber architecture is maintained after being processed by the microchannel EHD co-jetting device, even at flow rates of 26.4 ml hr^{-1}. B) A representative cross sectional view of the fibers shown in (A) highlights the two compartments present within the fibers. C) Scanning electron microscopy of fibers produced from 2 to 26.4 ml hr^{-1} show a bead free morphology which is similar at each respective flow rate. D) A histogram of fiber diameters from fibers spun in a standard side-by-side capillary (SEM shown in inset) is compared to the fiber size distributions of the fibers produced using the microchannel EHD co-jetting device at different flow rates, as indicated by the respective lines. E) Average fiber diameter is shown for each of the samples, showing the fiber size is consistent for each condition. Error bars indicate standard deviations. Scale bars indicate 10 μm (A-D).

A novel needle-less electrohydrodynamic co-jetting technique allows for the preparation of particles and fibers with two distinct compartments. Application of a high electric field results in the spontaneous formation of several distinct Taylor cones along a fluid interface, resulting in the deposition of bicompartmental fibers and particles. Production rates of fibers are more than 30 times higher than needle-based co-jetting methods.

Jacob H. Jordahl, Stacy Ramcharan, Joerg Lahann[*]

Needle-less electrohydrodynamic co-jetting of bicompartmental particles and fibers

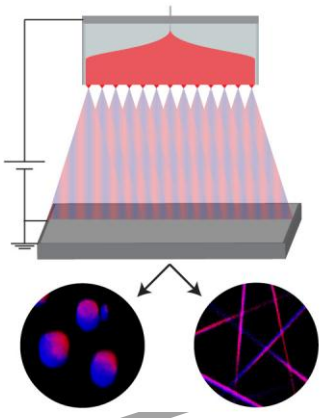

((Supporting Information should be included here for submission only; for publication, please provide Supporting Information as a separate PDF file.))

Supporting Information

for *Macromol. Rapid Commun.*, DOI: 10.1002/marc.2013#####

Needle-less electrohydrodynamic co-jetting of bicompartmental particles and fibers

Jacob H. Jordahl, Stacy Ramcharan, *Jason V. Grergory,* Joerg Lahann*

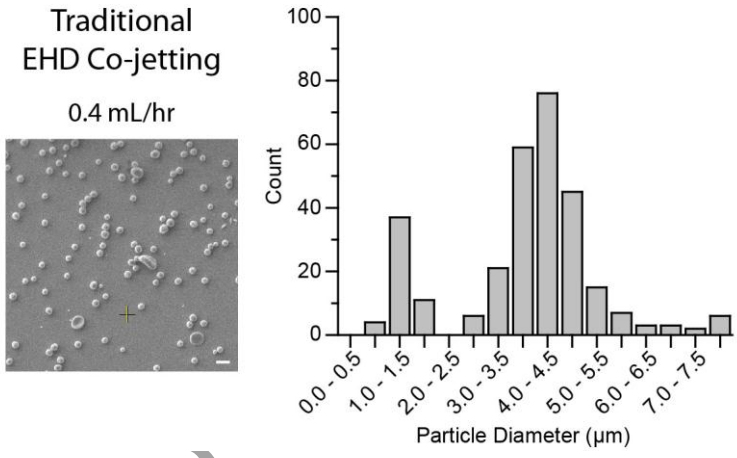

Figure S1. Microparticles fabricated using traditional EHD co-jetting technique. Parallel capillaries were utilized to obtain bicompartmental particles. A stable cone-jet is obtained at 0.4 ml hr^{-1}, and produces particles of a similar morphology and particle size distribution as particles fabricated using the needle-less high-throughput co-jetting device (Figure 3).

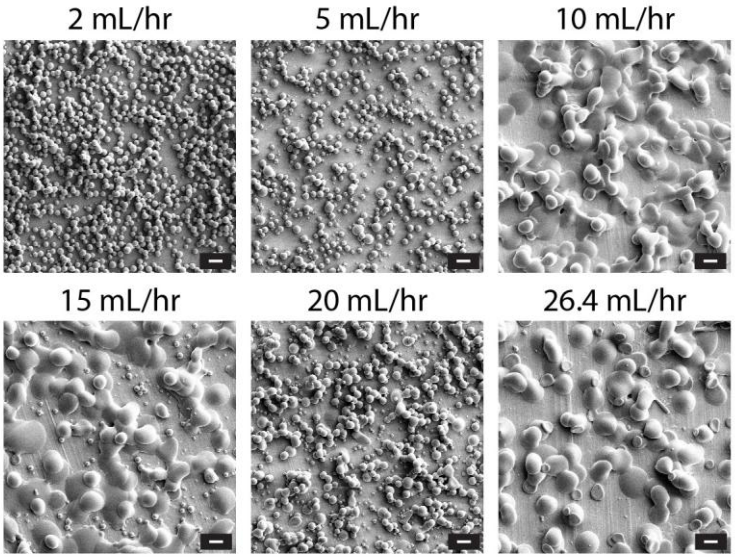

Figure S2. The effect of flow rate on resultant particle morphology. At flow rates of 2.0 to 5 ml hr^{-1}, particles with a spherical morphology were produced. At flow rates between 10 and 20 ml hr^{-1} a mixture of spherical particles and flattened disc morphologies were observed. The 26.4 ml hr^{-1} flow rate contained both discs and red blood cell shaped particles. Scale bars indicate 10 µm.

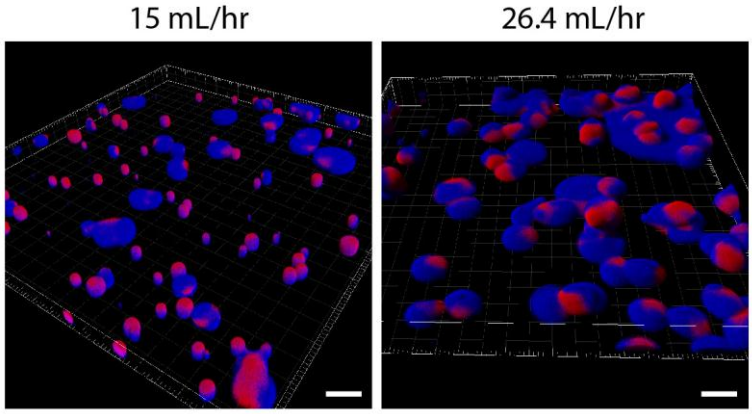

Figure S3. Bicompartmental particle architecture is maintained at higher flow rates despite different particle morphologies. At 15 ml hr^{-1} a combination of bicompartmental particles and discs were fabricated. Similarly, bicompartmental discs were observed at 26.4 ml hr^{-1} flow rates. Scale bars indicate 20 µm.

Movie S1. Demonstration of the device operation during fabrication of bicomponent PLGA/PVAc fibers at a flow rate of 26.4 ml hr^{-1}, collector distance of 40 cm, and applied voltage of 75 kV.

Movie S2. Deposition of the resultant bicomponent PLGA/PVAc fibers on the collection electrode at a flow rate of 26.4 ml hr^{-1}, collector distance of 40 cm, and applied voltage of 75 kV.